J Mater Sci (2011) 46:6029–6045
DOI 10.1007/s10853-011-5565-x

Preparation and characterisation of cellulose nanofibres

E. H. Qua · P. R. Hornsby · H. S. S. Sharma · G. Lyons

Received: 11 November 2010 / Accepted: 16 April 2011 / Published online: 7 May 2011

Abstract Two different procedures were compared for the preparation of cellulose nanofibres from flax and microcrystalline cellulose (MCC). The first involved a combination of high energy ball milling, acid hydrolysis and ultrasound, whilst the second employed a high pressure homogenisation technique, with and without various pretreatments of the fibrous feedstock. The geometry and microstructure of the cellulose nanofibres were observed by SEM and TEM and their particle size measured using image analysis and dynamic light scattering. Aspect ratios of nanofibres made by microfluidisation were orders of magnitude greater than those achieved by acid hydrolysis. FTIR, XRD and TGA were used to characterise changes to chemical functionality, cellulose crystallinity and thermal stability resulting from the approaches used for preparing the cellulose nanofibres. Hydrolysis using sulphuric acid gave rise to esterification of the cellulose nanofibres, a decrease in crystallinity with MCC, but an increase with flax, together with an overall reduction in thermal stability. Increased shear history of flax subjected to multiple passes through the microfluidiser, raised both cellulose nanofibril crystallinity and thermal stability, the latter being strongly influenced by acid, alkaline and, most markedly, silane pretreatment.

E. H. Qua · P. R. Hornsby (✉)
Polymers Cluster, School of Mechanical and Aerospace Engineering, Queen's University Belfast, Ashby Building, Stranmillis Road, Belfast BT9 5AH, UK
e-mail: peter.hornsby@qub.ac.uk

H. S. S. Sharma · G. Lyons
Applied Plant Science Division, Agri-Food and Bioscience Institute, Newforge Lane, Belfast BT9 5PX, UK

Introduction

Several recent reviews have documented current understanding on the preparation of cellulose nanofibrils, also known as cellulose nanofibres and nanowhiskers, and potential applications for these materials, including their use as polymer reinforcements [1–3]. A cellulose nanofibril has a needle-like structure, with nano-scale dimensions. Its diameter and length are generally below 30 nm and above 100 nm, respectively, exact dimensions depending on the fibre source and extraction method. As a result of their size, in low concentrations, a suspension of cellulose microfibrils is generally gel-like and transparent. Various values have been reported for the crystal modulus of cellulose ranging from 100 to 220 GPa depending on the assumptions made [1], which together with the high aspect ratio of cellulose nanofibres, has generated a number of studies aimed at investigating their reinforcing potential in a range of polymers [4–12].

Cellulose nanofibres have been formed from diverse sources including microcrystalline cellulose (MCC) [13–17], bacterial cellulose [18, 19], sugar beet primary cell wall cellulose [13, 20], cotton [21], tunicate cellulose [21, 22], ramie [23] and softwood pulp [24, 25].

Acid hydrolysis has been widely applied to isolate cellulose nanofibres from different cellulosic sources by breaking down their hierarchical structure This extraction method was first developed by Rånby and Ribi (1950), who prepared a stable suspension of colloidal-sized cellulose nanocrystals from cotton and wood using sulphuric acid hydrolysis [26, 27]. Subsequently there have been many related approaches reported [28–32]. It has been shown that the hydrolysis conditions, including reaction time, acid-to-pulp ratio and acid type have a great influence on the dimensions and surface charge of the cellulose nanofibres.

For example, a long reaction time and high acid-to-pulp ratio resulted in the formation of shorter and finer fibres [25, 33]. Surface charge present on the cellulose was found to depend on the type of acid used. Sulphuric acid provided a highly stable aqueous suspension with the introduction of sulphate groups on the surface of crystallites, whereas hydrochloric acid yielded minimal surface charge on the cellulose nanofibres [34, 35]. One of the major challenges when using acid hydrolysis to form cellulose nanofibres is to increase the final yield after processing, typically around 30% (of initial weight), which potentially limits scale-up by this method [14].

Through the application of shear and pressure, mechanical and chemo-mechanical treatment methods can also be applied to isolate nanofibres from plant fibre yielding so-called microfibrillated cellulose (MFC). This is defined as cellulose fibril aggregates obtained through disintegration of the cell wall in cellulose fibres [34]. MFC was first prepared by Turbak and Herrick, who defibrillated wood pulp cell wall using a conventional high shear homogeniser [35, 36]. Subsequently there have been many related reports using this approach [20, 37–40]. In the past, MFC was originally produced without the use of chemical treatments. Today, the term MFC refers to the desired final cellulose nanofibre being microfibrillar in nature even though a chemical method may be used [41]. The diameter of MFC fibrils is usually at the range of 10–100 nm and can be up to several micrometres in length, depending on the preparation methods and material source.

This article compares the preparation of cellulosic nanofibres from MCC and flax fibres, using two different approaches: a modified acid hydrolysis method and a high shear homogenisation technique. Particular emphasis is given to the physical and chemical characterisation of these fibres together with their thermal stability, in order to define their suitability as potential reinforcements for polymers.

Experimental

Materials

Microcrystalline cellulose (Asahi Kasei Chemicals Corporation, Japan) and flax fibre roving (Linavabrik, Estonia) were chosen as cellulose feedstock sources. The average fibre length of the MCC was reported as approximately 50 μm [26]. Sulphuric acid (98%) was obtained from Sigma-Aldrich Chemical Co. Ltd. Typically flax fibre comprises 64.1% cellulose, 16.7% hemicellulose, 1.8% pectin, 2% lignin, 3.9% water soluble, 1.5% wax and 10% water [42]. However, the chemical composition can be influenced by the climatic conditions, maturity and retting process [43–45]. For the material under investigation the caustic weight loss was 20.3%, ash content 0.5%, carbon content 41.85% and nitrogen content 0.33%.

Preparation of cellulose nanofibres

Chemical treatment

Preparation of cellulose microfibrils from these sources involved a combination of acid hydrolysis, ultrasonic and high energy ball milling techniques. Flax fibres were first cut manually to a length between 20 and 30 mm, before milling using a high energy ball mill (PM100 series from Retsch UK) at 600 rpm for 2 h. MCC and flax fibres were then hydrolysed according to the conditions given in Table 1. The mixture was centrifuged up to 5 times to remove the excess acid (10 min at 9,500 rpm), then exposed to ultrasonic energy (VWR® Ultrasonic Cleaner Model 150 T, 150 W) for 30 min. The supernatant was removed from the sediment and replaced by distilled water to stop the hydrolysis reaction. The centrifugation steps were repeated until the supernatant became turbid, before dialysis against tap water for 2 days until the suspension reached a pH of 7. This was then passed through a Whatman 41 grade quantitative filter paper to remove any remaining micro-particles. The final concentration of the suspension was then increased to 1 wt% solids using a Rotavapor at 40 °C for approximately 1 h (depending on water content). The cellulose suspension was then cast on a petri disc and dried at ambient temperature for 5 days. The resulting cellulose films were subsequently dried further in an oven at 70 °C for 2 days, prior to characterisation. The samples derived from flax fibres with a length of between 20 and 30 mm and ground flax fibres were designated as flax nanofibre and flax nanofibre (powder), respectively.

High pressure homogenisation

Cellulose nanofibres were also produced from flax fibre using a high pressure homogenisation procedure. The starting feedstock was first ground into a powder using a cryogenic grinder (Spex 6850 freezer, Spex CertiPrep, UK) in nitrogen for 20 min. Using this powder, fibrous pulps were prepared in water at 0.5 wt% concentration, with some receiving acid, alkaline or silane pretreatment. Hydrolysis was undertaken using 20 wt% sulphuric acid for 20 min at 25 °C using an acid:pulp ratio of 20:1. Mercerisation was carried out with an 18 wt% aqueous concentration of sodium hydroxide for 1 h at 25 °C and a 20:1 alkali:pulp ratio. After treatment, these materials were neutralised with running water to a pH of 7. Silylated cellulose nanofibres were also prepared using 3-glycidoxypropyltrimethoxysilane (Dynaslan® GLYMO, Degussa)

Table 1 Hydrolysis conditions used for preparation of MCC and flax nanofibres and the yields (% of initial weight) after various treatments

	Source	Acid hydrolysis				Ball milling	Ultrasound	Yield (wt%)
		Acid (wt%)	Temp (°C)	Time (min)	Acid:pulp			
Run 1	MCC	60	45	130	10	–	No	25
Run 2	MCC	60	45	130	10	–	Yes	45
Run 3	Flax	64	60	50	20	–	No	42
Run 4	Flax	64	60	50	20	–	Yes	N/A
Run 5	Flax	64	60	50	20	Yes	No	38
Run 6	Flax	64	60	50	20	Yes	Yes	N/A

Acid, sulphuric acid concentration in weight percent (acid hydrolysis), *Temp*, reaction temperature (acid hydrolysis), *Time*, reaction time (acid hydrolysis), *Acid:pulp*, the ratio of acid to fibre pulp (acid hydrolysis), *Ball mill*, ball milling process, *Ultrasound*, ultrasonic treatment

dissolved at in the suspension at a 2 wt% concentration before the homogenisation process.

Two microfludizers M110Y and M110EHI with different pressure ratings were employed to prepare cellulose nanofibres. M110-Y is a portable laboratory unit that provides high shear rates, using high pressure (max. 1586 bar), with a flow rate range of 250–600 mL/min and 60 mL sample size. The M-110EHI facility can operate at higher pressures up to 2,070 bar, with a flow rate up to 320 mL/min and maximum sample size of 120 mL. With each machine the material was recycled up to 80 times. Most samples were prepared using a microfluidiser pressure of 1000 bar, but some untreated materials were produced at a higher pressure of 1800 bar.

The following sample designation was used: F, flax; C, control; 5P, 20P, 50P, 80P, number of passes through microfluidiser; A, acid pretreatment; N, alkaline pretreatment; S, pretreatment with silane. H, higher pressure use (1800 bar).

For example: FS-50P refers to silane pretreated flax passed through the microfluidiser 50 times.

Gravimetric analysis

The concentration of cellulosic nanofibres was measured by weighing a small amount of suspension before and after water evaporation. The values were obtained from an average of three measurements. Nanofibre concentration was determined as a percentage of initial weight.

FTIR analysis

A Perkin Elmer (Spectrum 1000) spectrophotometer was used to characterise dried cellulose samples. For this purpose samples were either ground to a powder and a small quantity (approximately 1 mg) blended with 300 mg of KBr powder and compressed to form a disc, or analysed directly in a universal ATR sampling accessory. The spectrum for each sample was recorded as an average of 100 scans at a resolution of 2 cm^{-1} in the range from 4000 to 500 cm^{-1}. Each sample was tested in triplicate.

Morphology

The morphology, diameter and length distribution of cellulose nanofibres were studied using a medium resolution Philips CM100 transmission electron microscope (TEM) at a voltage acceleration of 100 kV. A droplet of suspension was placed on a Cu-grid and coated with a thin film of carbon. To improve contrast, the cellulose nanofibres were stained with a 1 wt% solution of uranyl acetate for 30 s. The sample was then immersed in distilled water to remove excess treatment, before drying at ambient temperature. Surface morphology of resulting cellulose films was also examined using a JEOL JSM-6500F scanning electron microscope (SEM). Samples were sputter coated with gold to avoid build up of electrostatic charge.

X-ray analysis

X-ray diffraction patterns of powdered cellulose nanofibres were obtained at 40 kV and 40 mA using an X'pert Pro Panalytical, X-ray diffractometer. The samples were scanned at a rate of 0.03 step/0.6 s using a Ni-filtered Cu Kα beam (wavelength, $\lambda = 1.5406$ Å). Multiple scans were undertaken on each sample.

Particle size analysis

Static image analysis

Jmicrovision 1.25 software was used to measure the diameters and lengths of particles from two dimensional images obtained from TEM micrographs. At least 700 particles were examined to achieve the mass-median diameter within a 10% error with 95% probability for nanoparticles having a maximum of 1.50 geometric standard deviation. Particle size results were reported according to ISO 13322-1:2004.

Laser diffraction (dynamic light scattering)

The particle size distribution of nanofibre suspensions was measured using a Zetasizer ZS series DLS from Malvern Instruments, England. For this purpose a 1 wt% aqueous suspension of cellulose nanofibres was examined according to ISO 13320-1:1999. At least five different measurements were undertaken from each sample.

Thermal analysis

A microbalance and furnace unit (STA 851e with TSO 80 RO sample robot) was used to determine the thermal stability of the fibre-reinforced polymer, untreated and treated samples. Typically sample sizes were between 5 and 10 mg. Weight loss and first derivative of weight loss were recorded using Mettler STAR software. Each sample was tested in triplicate and averaged, over a temperature range from 30 to 600 °C at a heating rate 20 °C/min in a nitrogen environment.

In order to identify decomposition products from the cellulose nanofibres, TG-MS analysis was performed on selected samples using a Mettler Toledo TGA/SDTA851 thermal analysis system, equipped with an autosampler and TSO801RO sample robot, coupled to a Pfeiffer vacuum thermostar quadrupole mass spectrometer (Pfeiffer Vacuum), equipped with a QME Prisma detector and operated in electron impact ionisation mode at 70 eV. Evolved gases passed from the TGA to the mass spectrometer via a heated silica capillary (0.22 mm of inner diameter) maintained at 180 °C. 4.5 mg of each sample was heated in alumina crucibles (150 μL) from room temperature to 650 °C at a heating rate of 10 °C/min and nitrogen purge gas flow of 50 cm^3/min. The MS signal range was monitored from 10 to 95 m/z.

Results and discussion

Appearance and yield

The cellulose nanofibres suspensions made by chemical treatment were gel-like or transparent depending on concentration, having a white tint, when derived from MCC and light brown when using flax fibres, indicating the presence of residual organic substrates, including lignin, in this material. The percentage yield of cellulosic nanofibres obtained from the various chemical preparation alternatives is shown in Table 1. The yield of nanofibres from MCC after acid hydrolysis of MCC (Run 1) was only 25%, which is slightly lower than the value reported by Bondeson [14]. This is may be attributed to the lower centrifuge speed (9,500 rpm) used during preparation, which resulted in removal of some nanofibres along with the acid. The significant increase in yield of nanofibres from Run 2 is considered to result from the enhanced isolation of nanofibres after exposure to ultrasound. This procedure creates cavitation and high vibrational energy in the suspension, resulting in the separation of cellulose nanofibre bundles and agglomerates [46].

With the high energy ball mill, the yield obtained from powdered flax was lower than that derived from the fibrous variant. This is thought to result from the increase in surface area available for acid digestion of the crystalline component, as the particle size was reduced and is also reflected in the XRD results discussed later, which suggests a lower crystalline content in nanofibres prepared from powdered flax. Similar observations were reported by Caulfield [47], who observed that that ball milling enhanced the enzyme digestibility of the crystalline component, as a result of the reduced particle size. Although ultrasonic treatment increases the yield of nanofibres, the appearance of aggregates and flocculation (at 0.5 wt% suspension concentration) was observed with Runs 4 and 6 (using flax fibres). This may be attributed to the presence of residual, hemicellulose, lignin and pectin in the flax fibre.

From visual observation of the cellulose suspensions produced from flax fibres subjected to high pressure homogenisation, it was apparent that with alkali treated fibres (FN-$5P^b$), increasing the number of passes through the microfluidizer resulted in increased fibre dispersion and homogeneity. However, this was less evident with the preparation alternatives.

Morphology and particle size distribution

Representative TEM images showing the morphology of nanofibres prepared from MCC and flax fibres by acid hydrolysis, using conditions identified in Table 1, are compared in Fig. 1. The rod-like geometry of the cellulose nanofibres apparent was similar to that seen in previous studies [1–3]. An estimate of the aspect ratio of the nanofibres prepared was made by image analysis, using Jmicrovision software. The number of particles measured was determined by the specified confidence limits recommended in ISO 13322-1:2004. Size distributions for the length and diameter of nanofibres obtained from MMC and flax by this method are compared in Fig. 2. From these results, MCC cellulose nanofibres were found to have lengths (L) ranging from 21 to 300 nm and diameters (D) from 2 to 22 nm (Table 2). The average values of L and diameter D are 111 ± 43 and 8 ± 2 nm, respectively. Cellulose nanofibres derived from flax fibres had lengths ranging from 21 to 350 nm and diameters from 2 to 50 nm. In this material, the average values of L and D were found to be 9 ± 5 and 141 ± 57 nm. Nanofibres produced

from powdered flax had a length range from 21 to 340 nm and diameters ranging 2–18 nm. Hence, the average values are only 7 ± 2 and 122 ± 49 nm. Therefore, the average aspect ratio (*L*/*D*) of flax nanofibre, flax nanofibre (powder) and MCC nanofibre were very similar being approximately 17, 17 and 14, respectively.

The changes in physical structure of the flax fibres induced by high pressure microfluidisation are shown in Figs. 3 and 4. It is clear that the method of sample preparation, whereby the nanofibre suspensions were dried before examination on the SEM, resulted in coalescence and the formation of a mat-like structure. Although the extent of fibre agglomeration may have masked differences in the effects of the treatment process, nevertheless some general conclusions can be drawn from these observations.

Overall, this refinement procedure leads to fibrous structures with diameters between 30 and 100 nm and estimated lengths of several tens of micrometres, resulting in very much higher aspect ratio nanofibrils than was achieved by acid hydrolysis. For the untreated flax fibre pulp, the content and size of nanofibrils in the suspension decreased with increasing number of passes through the homogeniser, resulting in a greater tendency for the nanofibrils to interact and agglomerate.

Finer and shorter fibrils were expected in the samples from a combination of sulphuric acid pretreatment and high pressure microfluidisation, however, this was not obvious from the SEM micrographs shown in Fig. 4. This was attributed to the strong intermolecular hydrogen bonding, resulting in fibril agglomeration during the sample drying process. More insight into the particle size of these nanofibres in suspension was obtained through dynamic light scattering (DLS), as described later.

Since alkali treatment can lead to fibre fibrillation and swelling, this might be expected to generated higher friction and shear forces in the microfluidiser capillary, resulting in finer and shorter nanofibrils. Again this was not apparent in the SEM micrographs, as if anything, the fibrils were much coarser than the samples treated solely by mechanical means. This may be a consequence of the removal of hemicelluloses, wax and pectin from the flax fibres [48], increasing their purity, and resulting in stronger interaction between the cellulose chains, thereby reducing their tendency to fibrillate. However, it is also probable that finer fibrils were created, which then coalesced to obscure the extent of initial fibre breakdown. However, when sheared in the presence of the silane solution, there was a clear reduction in fibril diameter relative to fibrils obtained purely by mechanical means which again shows a decrease with increasing number of passes through the microfluidiser. Application of the silane treatment to the fibrils surface is considered to inhibit agglomeration, thereby yielding a more stable suspension during the homogenisation process and also limit coalescence when analysed in the SEM.

Using the M-110EHI Microfludizer at higher pressure (1,800 bar rather than 1,000 bar) fibril diameter was

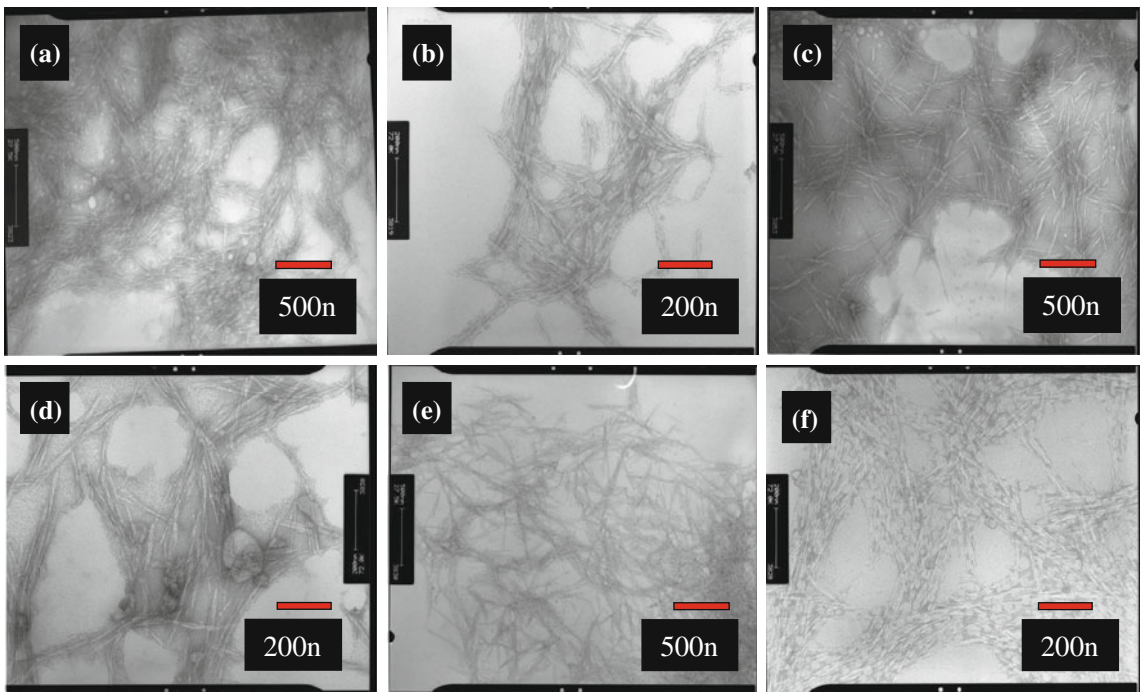

Fig. 1 TEM micrograph of cellulose nanofibres from Run 2 (**a**, **b**), Run 3 (**c**, **d**) and Run 5 (**e**, **f**). Run 2: MCC with acid hydrolysis and ultrasonic treatment, Run 3: flax fibre with acid hydrolysis only and Run 5: flax fibre with ball milled and acid hydrolysis

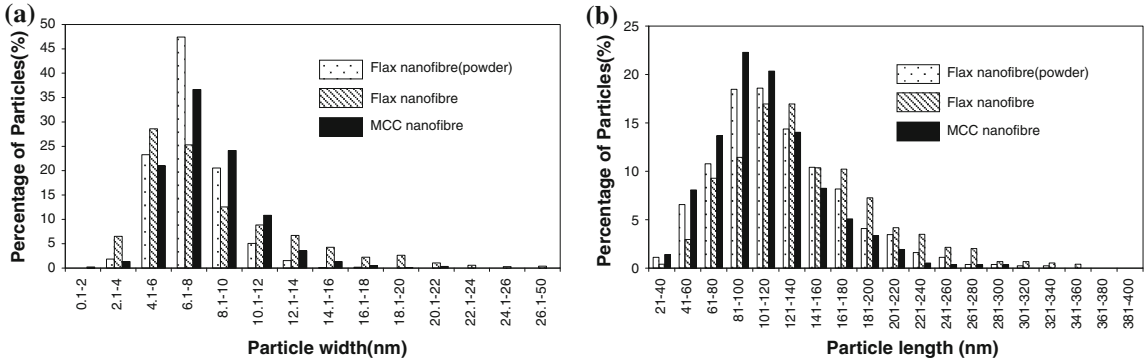

Fig. 2 Size distribution of cellulose nanofibres made by acid hydrolysis: **a** width (diameter) and **b** length

Table 2 Average particle size, standard deviation, error and aspect ratio of cellulose nanofibres derived from flax fibres and MCC

	MCC nanofibres	Flax nanofibres (powder)	Flax nanofibres
Diameter, *D* (nm)			
Mean	7.9	7.2	8.5
Standard deviation	2.4	1.6	4.5
Error (mass-median)	0.2	0.1	0.2
Error (mean-volume)	0.1	0.1	0.1
Length, *L* (nm)			
Mean (nm)	110.7	122.2	141.2
Standard deviation	42.6	49.3	57.4
Error (mass-median)	0.3	0.3	0.3
Error (mean-volume)	0.1	0.1	0.1
Aspect ratio, *L*/*D*	14.0	16.9	16.6

significantly reduced, relative to material made at a lower pressure (Fig. 3), due to the higher apparent shear rate developed through the capillary. Thus, the fibrillated structure obtained from sample FH-50P was broadly similar to F-80P. The fine distribution of these nanofibrils in sample FH-40P, is clearly shown in Fig. 5 and in corresponding particle size distribution results, discussed below.

Dynamic light scattering

Although analysis from TEM micrographs gives useful information regarding nanofibre geometry, the accuracy of measurements is limited by the small fraction of particles analysed relative to the whole sample. Hence, to evaluate the particle size of the samples more fully, a DLS method was also employed. Nevertheless, such measurements are strongly influenced by a number of factors. Firstly, DLS measures the hydrodynamic radius of spherical particles. With DLS, particle size is determined from the Einstein–Stokes relation and thus the rod-like fibres are treated as spherical particles, which is clearly far from reality [48]. Since, the principle of DLS is based on the measurement of the scattered light intensity caused by Brownian motion of particles in solvent without applying an electric field [45, 49, 50], this poses a challenge for the measurement of particles with a high aspect ratio since the length determined is influenced the diameter of the nanofibre. Hence, the particle size evaluated must be larger than the real dimensions of particles [46] and the sizes obtained from DLS are likely to be different to those measured by image analysis. In addition, the hydrodynamic radius of the 'spherical' particles will depend the extent of particle–particle interactions when present in an aqueous suspension. This will be strongly influenced by the concentration particles in the system, and the potential effects of modification of the fibre on their surface chemistry and resulting hydration shells. It is important to note, therefore, that the data derived from DLS does not give absolute values for the size of cellulose nanofibre, but does allow differences between the samples made under changing processing conditions to be compared, as described in this study [46, 51].

Results from DLS determinations are shown in Figs. 6, 7 and 8, in terms of percentage intensity, rather than number, against particle size. It should be noted that there are two methods for calculating zeta particle size either using a cumulant algorithm or a distribution algorithm. The latter method has been applied in this work, which involves analyzing the autocorrelation function using an inverse Laplace transform known as CONTIN [52, 53]. This

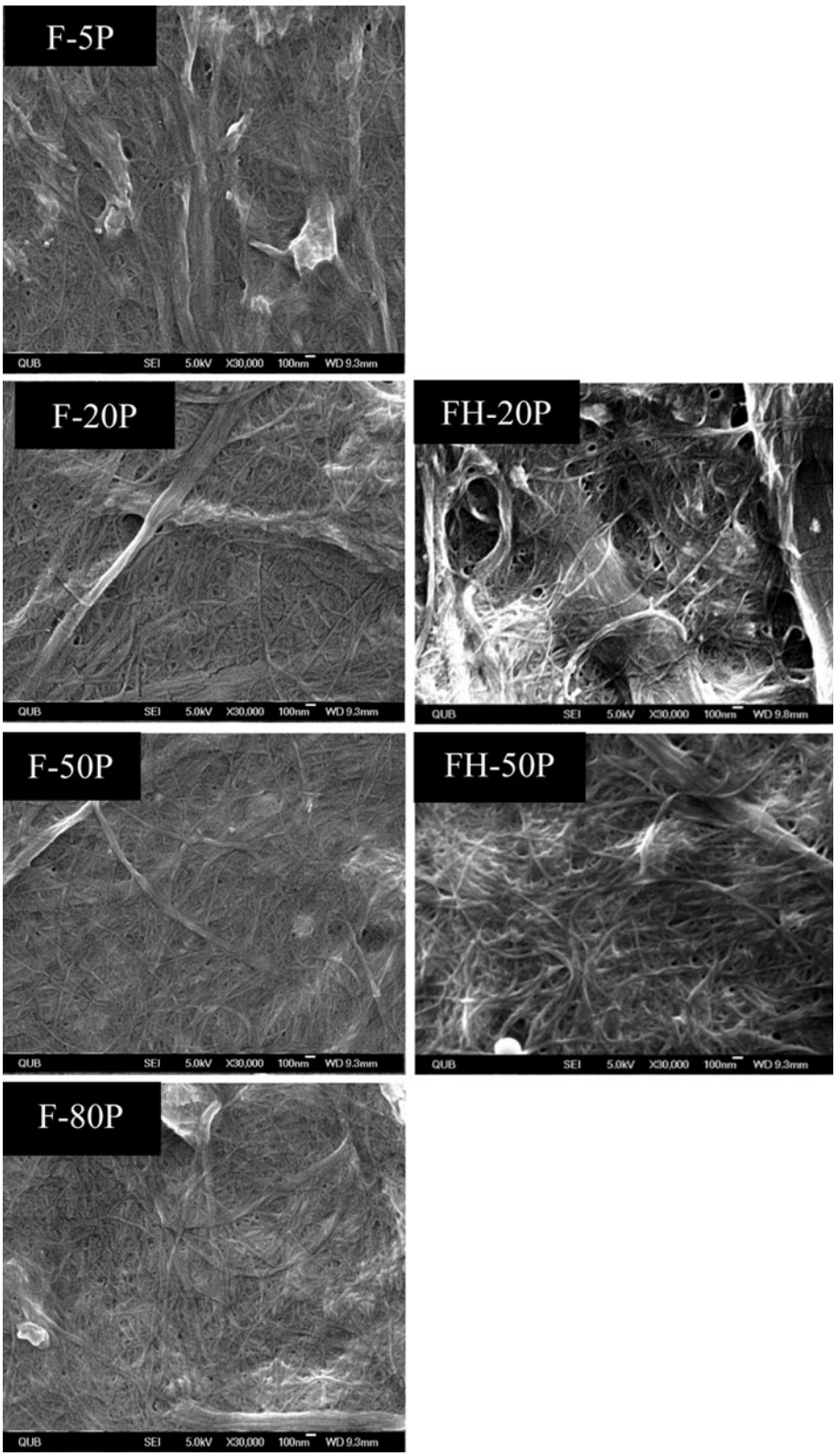

Fig. 3 SEM micrographs of the defibrillated flax fibres after multiple passes through microfluidiser at 1000 bar (F) and 1800 bar (FH)

analysis is ideal for polydisperse and multimodal systems which cannot be resolved by the cumulant method. The resolution for separating two different particle populations is approximately a factor of five or higher and the difference in relative intensities between two different populations should be less than 1×10^{-5}. It should be noted that DLS results presented in this work using the distribution algorithm method are represented as multiple

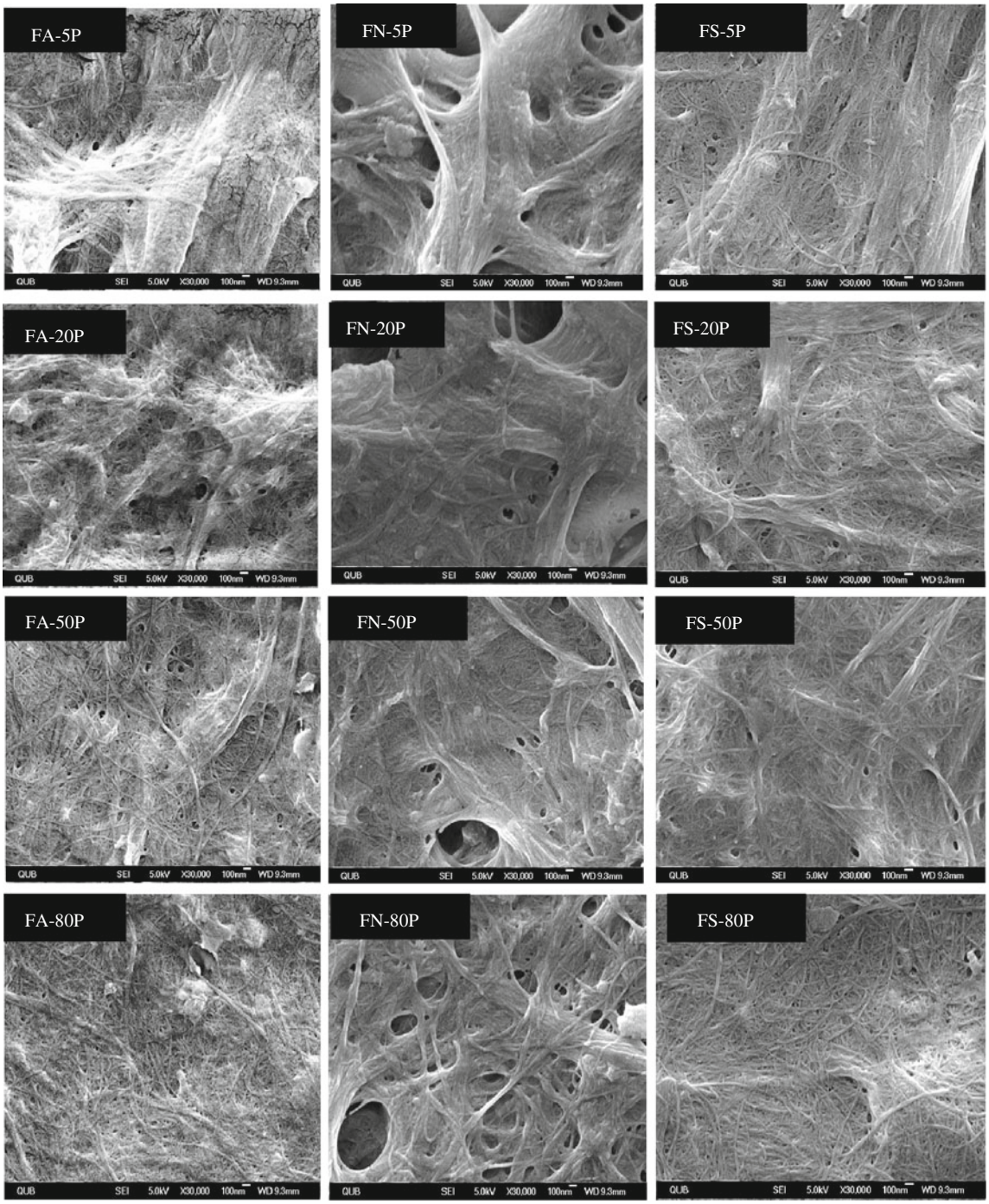

Fig. 4 SEM micrographs of the defibrillated flax fibres after multiple passes through microfluidiser at 1000 bar. *FA* acid treatment, *FN* alkaline treatment, *FS* silane treatment

peaks. These are believed to be real phenomena arising from natural variation and compositional differences in the starting materials. Also, these results are shown as raw data, with no attempt made to filter out components with widely differing particle size.

Figure 6 shows the light scattering intensity distribution of the nanofibre samples produced by acid hydrolysis. From this result three groups of particles with different size ranges are presented in Table 3. This shows that MCC nanofibres have lengths ranging from 16 to 142 nm and diameters from 5 to 7 nm. Cellulose nanofibres derived from flax fibres have lengths from 44 to 615 nm and diameters from 14 to 24 nm, whereas with the nanofibres made from powdered flax lengths ranged from 38 to 396 nm and diameters from 9 to 16 nm. Using this method for nanofibres produced by acid hydrolysis, particle size

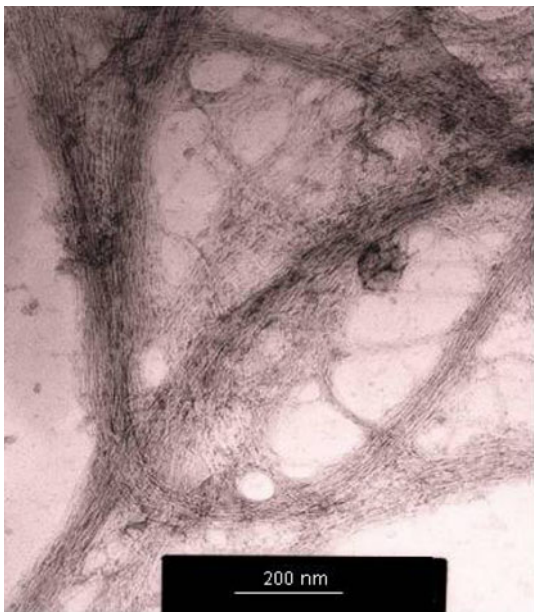

Fig. 5 TEM micrograph of FH-40P produced on microfluidiser

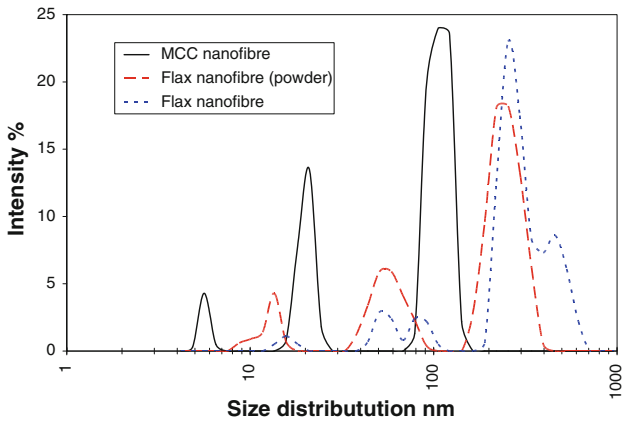

Fig. 6 Size distribution of cellulose nanofibres produced by acid hydrolysis determined by DLS

measured showed the following trends: MCC nanofibre < flax nanofibre (powder) < flax nanofibre, which was also verified by image analysis.

The particle size distribution of these samples derived from the microfluidisation homogenisation process was also studied using DLS. However, again it should be noted, however, that due to the greater aspect ratio of these fibres, relative to those made by chemical treatment, absolute measurement by this technique is even more subjective. Nevertheless, relative differences were apparent depending on the preparation conditions used and surface modification applied.

Fibrils with diameters below 100 nm and high aspect ratio could be isolated from flax fibres by purely mechanical treatment. Due to the method used for presenting the

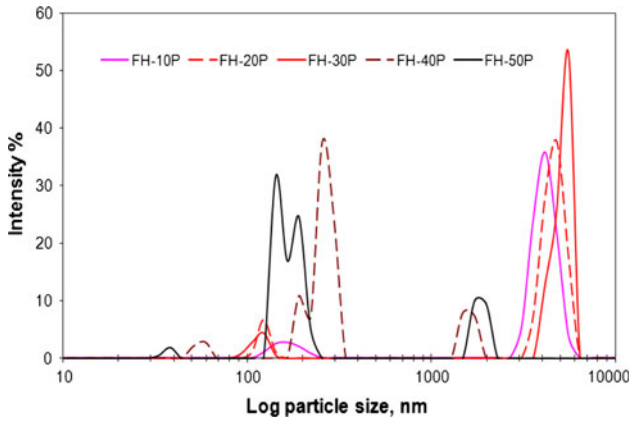

Fig. 7 Size distribution of cellulose nanofibrils (without pretreatment) after multiple passes through microfluidiser M110-EHI at 1800 bar

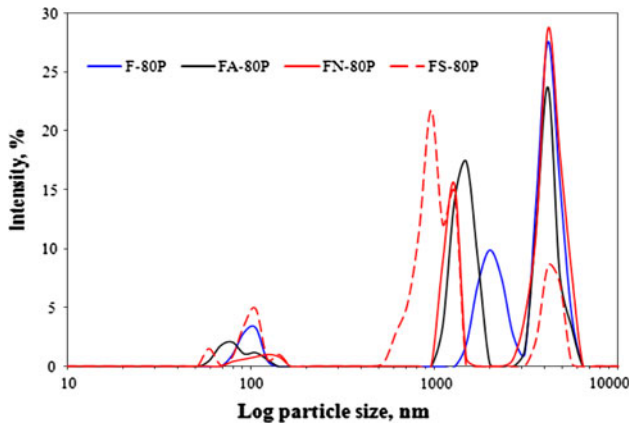

Fig. 8 Size distribution of cellulose nanofibrils (with and without pretreatment) after 80 passes through microfluidiser M110-Y at 1000 bar. *F* no treatment, *FA* acid pretreatment, *FN* alkaline pretreatment, *FS* silane pretreatment

data, discussed above, DLS results generally gave two or three peaks (see Fig. 7, for example). The size distribution of the cellulose nanofibrils made at 1000 bar followed the order: F-5P > F-20P > F-50P > F-80P, which concurs with the trend seen in the SEM micrographs (Fig. 3), and diameter distribution of fibrils determined in other studies. For example, Zimmermann [39] obtained high aspect ratio fibrils with diameters below 100 nm using an Ultra-Turrax homogeniser and a microfluidizer. Taniguchi and Okamura [40] also obtained fibrils with diameters in the range of 20–90 nm from wood pulp using a high intensity grinding method. Turbak [35] and Herrick [36] used a Gaulin high pressure homogeniser to produce MFC with a diameter range between 25 and 100 nm.

As shown in Fig. 7, as expected, the diameter distribution of fibrils derived at higher pressure (1800 bar) also decreases with number of passes, due to the greater defibrillation of the fibres resulting from the much higher shear

Table 3 Size ranges of cellulose nanofibres made by acid hydrolysis and determined by DLS

Source	1st Group	2nd Group	3rd Group
MCC nanofibre (nm)	5–7	16–24	79–142
Flax nanofibre (powder) (nm)	9–16	38–79	164–396
Flax nanofibre (nm)	14–24	44–91	190–615

developed. In fact the diameter distribution of FH-50P obtained from DLS was much smaller than F-50P, again showing the strong pressure dependency of the process. The effects of pretreatment prior to microfluidisation, also has a significant influence on nanofibril size. Acid modification yielded finer and shorter fibrils of a similar size to those determined in related studies (Fig. 8) [39]. In this earlier work pulp treated with 10 wt% sulphuric acid at 60 °C for 16 h yielded fibril diameters below 50 nm. There was also a dependency on acid concentration, treatment time, disintegration time and number of passes, as seen in the present study. Alkaline pretreatment prior to mechanical shearing did not show the same effect on fibril breakdown, however, with less sub 100 nm material being produced than the other conditions used (compared after 80 passes in Fig. 8). Furthermore, the corresponding micrographs (see Fig. 4) suggest the presence of greater amounts of unfibrillated material.

It is clear, however, both from the DLS and SEM results (Figs. 8, 4) that pretreatment with 3-glycidoxypropyltrimethoxysilane gave significantly finer nanofibrils than the other conditions used. Again, there was a clear effect of the magnitude of shear history on the ultimate size of the particles obtained. The principal reason for applying the silane solution was to coat the nanofibres during fibrillation to give effective surface coverage on the new surfaces as they are created, and hence provide a means for enhancing fibre/matrix interaction in polymer composites subsequently made from these materials. However, this treatment also appears to aid the fibrillation process and stabilise the nanofibres from reagglomeration.

Fourier transform infrared spectroscopy

Analysis of FTIR spectra for MCC and MCC nanofibres made by acid hydrolysis at wavenumbers between 4000 and 450 cm^{-1} showed that with the nanofibre, there was a significant decrease in peak intensity at 3400 and 2894 cm^{-1}, corresponding to vibration of OH···O hydrogen bonding and antisymmetric and symmetric vibration of CH_2 groups, respectively. Peaks at 1445, 1364, 1120–1020, 895 and 660 cm^{-1}, corresponded to the in-plane deformation of CH_2, in-plane deformation of OH, vibration of C-O, rocking vibration of CH_2 and out of plane deformation of OH···O hydrogen bonding, respectively [54].

The intensity of most of the peaks is significantly decreased, or disappeared altogether after sulphuric acid hydrolysis, except for a band at 1645 cm^{-1} which corresponds to absorbed O–H and carbonyl bands in cellulose. The intensity of this absorption is influenced by oxidation of the cellulose during the acid hydrolysis reaction [55, 56]. The introduction of sulphate groups to MCC nanofibres resulted in a shoulder at 1210 cm^{-1}. This is due to the esterification of hydroxyl groups by sulphate ions from sulphuric acid treatment of cellulose [14] which also resulted in a significant reduction in the intensity of peaks at 3400 and 660 cm^{-1}.

Corresponding FTIR spectra for the flax fibre precursor and resulting nanofibre made by acid hydrolysis were similar to results for MCC, although there was a significant decrease in peak intensity at 3400 cm^{-1} for flax cellulose microfibrils. Otherwise, the flax fibres showed characteristic peaks at 3400 cm^{-1} (vibration of OH···O hydrogen bonding), 2894 cm^{-1} (antisymmetric and symmetric vibration of CH_2 groups), 1720 cm^{-1} (unconjugated C=O in hemicellulose), 1645 cm^{-1} (absorbed O–H or carbonyl band in flax fibre), 1510 cm^{-1} (aromatic rings of lignin), 1456 and 1424 cm^{-1} (C–H deformation in lignin and carbohydrates), 1370 cm^{-1} (C–H deformation in cellulose and hemicellulose), 1120–1020 cm^{-1} (vibration of C–O in cellulose and hemicellulose), 895 cm^{-1} (rocking vibration of CH_2) and 660 cm^{-1} (out of plane deformation of OH···O hydrogen bonding) [54, 57].

The disappearance of small sharp band at 1424 cm^{-1} and a general decrease in peak intensity at 1720 cm^{-1} was observed with the flax nanofibre. This indicates that most of the hemicelluloses and lignin have been extracted during the hydrolysis process. The shoulder in the region of 1210 cm^{-1} was observed for the flax nanofibre, which, as suggested for MCC nanofibre, corresponds to the stretching vibration of the sulphate group resulting from hydrolysis by sulphuric acid [58].

Additionally, ATR infrared analysis was undertaken on nanofibres prepared by high pressure shear modification, with and without chemical pretreatment and after multiple passes through the homogeniser. Figure 9 shows spectra of the flax nanofibrils without pretreatment, which shows similar absorptions characteristic of flax fibres, as identified above. When normalised, there is no significant difference in the intensity of characteristic peaks (for example at 3350, 2900, 1720 and 1645 cm^{-1}) resulting from multiple passes through the homogenisation process.

Acid hydrolysis and mercerisation of these cellulose nanofibrils gave essentially the same spectra to the untreated material after multiple passes, although complete disappearance or a decrease in intensity of the small sharp bands at 1720 and 1120 cm^{-1} was observed (Fig. 10). This suggests that most of the hemicellulose was removed

during these pretreatment procedures, since it has been reported that the attenuation of the vibration around 1720 cm^{-1} corresponds to the reduction of carbonyl groups present into fatty acids and C=O of nonconjunagated ketones, present in hemicellulose [48].

With silane pretreatment, the principal differences relative to the control are observed at between 800 and 900 cm^{-1} (indicated by circle), and strong peaks at 1030, 1102 and 1200 cm^{-1} (Fig. 11). The presence of two peaks near 800 cm^{-1}: 850 and 790 cm^{-1} are attributed to –S–CH_3 and the peak at 1030 cm^{-1} is associated with –Si–OH stretching [48, 59, 60].

In the presence of moisture, a silane converts to a silanol, which under appropriate conditions would be expected to covalently bond with hydroxyl groups on the fibres [61, 62]. The question remains whether in the present study silane interaction with the cellulose arises from hydrogen bonding, covalent bonding, or a combination of both. It has been reported that at 1030, 1055, 1110, and 1146 cm^{-1} are characteristic of –Si–O–Si– and –Si–O–C– bonds indicative of a chemical reaction between hydrolysed silane and, in this instance, hemp fibre, together with existence of a polysiloxane network [63]. Abdelmouleh [64], in a study of silane modified cellulose fibres, has assigned broad intense absorptions around 1200 and 1135 cm^{-1} to the stretching of –Si–O– cellulose and –Si–O–Si– bonds, respectively. Furthermore, it was also shown that after thermal treatment at 120 °C for 2 h under nitrogen, that these bands increased in intensity demonstrating that silane grafting had been enhanced.

Hence from inspection of Fig. 11 and the occurrence of absorptions at 1030, 1102 cm^{-1} and especially 1200 cm^{-1}, it is inferred that some silane grafting has taken place on the nanofibrils. The intensity of these absorptions increases with number of passes through the homogeniser, again reflecting the higher surface area of nanofibrils created and therefore greater silane coverage. Similarly there is also an indication that the presence of methyl groups in the silane intensifies the peak at 2900 cm^{-1}, especially after 80 passes through the microfluidiser. In this regard, a small decrease in intensity of the absorption at 1720 cm^{-1} suggests that hemicellulose present may also be involved in silane bonding during the microfluidisation process [57]. It is also evident that the peak near 2900 cm^{-1} for the unmodified flax fibre splits into two distinctive peaks at 2830 and 2930 cm^{-1} in the presence of silane.

X-ray diffraction

X-ray diffractograms for the cellulose nanofibres and their sources made by acid treatment are shown in Fig. 12. Three main reflections at $2\theta = 15.2°$, 16.8° and 22.6° were observed for both of the cellulose sources and nanofibres, corresponding to a cellulose I structure [8]. There was an increase in the intensity at 22.6° seen with flax nanofibre compared to its precursor. This indicates that the cellulose microfibrils derived from flax fibre are more crystalline than the source material. The lignin and polyose layer such as hemicellulose surrounding the flax fibres are first degraded by acid hydrolysis. Furthermore, amorphous regions in cellulose fibrils are penetrated and dissolved preferentially, proportionately increasing the content of crystalline material [8, 65, 66]. Conversely, the intensity of reflections for MCC nanofibres was significantly decreased

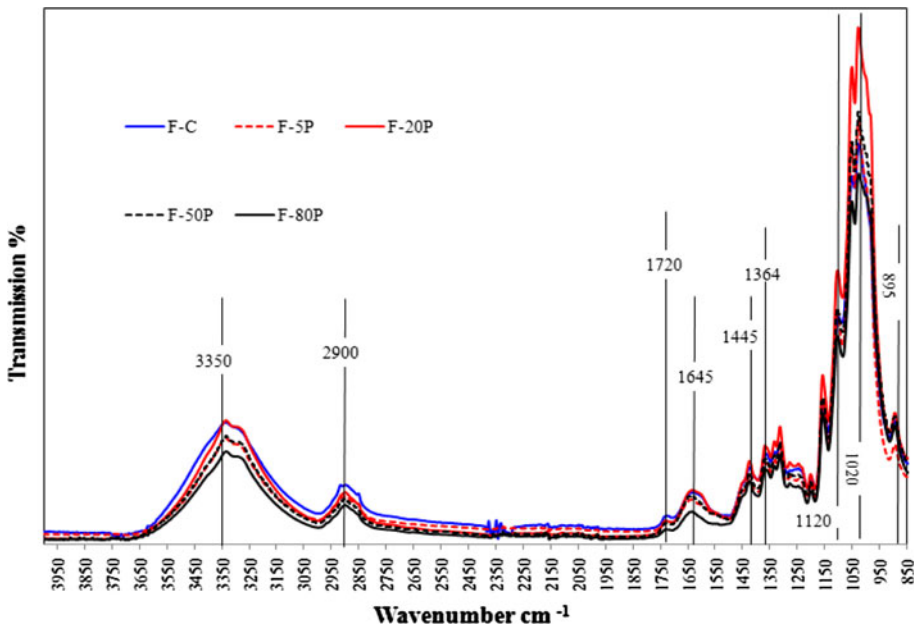

Fig. 9 FTIR spectra of flax control (FC) and flax nanofibrils (without pretreatment) after multiple passes through microfluidiser M110-Y at 1000 bar

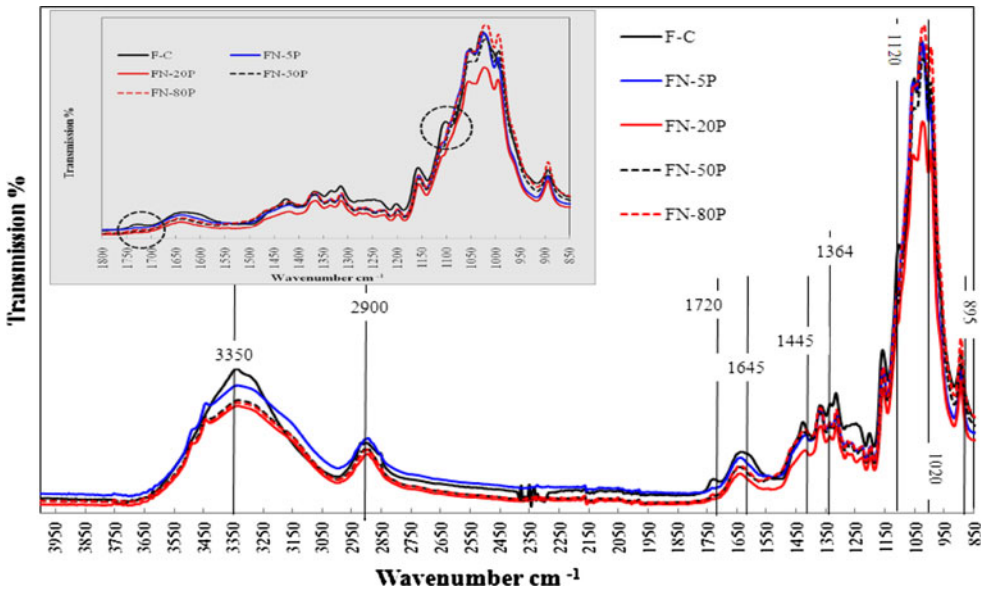

Fig. 10 FTIR spectra of flax control (FC) and flax nanofibrils (with alkaline pretreatment) after multiple passes through microfluidiser M110-Y at 1000 bar

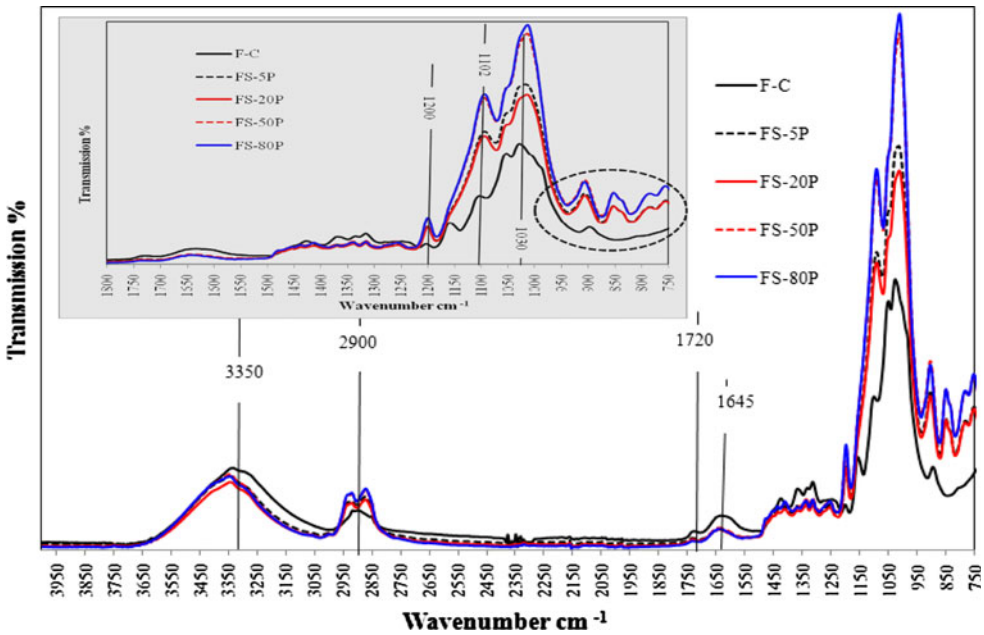

Fig. 11 FTIR spectra of flax control (FC) and flax nanofibrils (with silane pretreatment) after multiple passes through microfluidiser M110-Y at 1000 bar

relative to the parent material, suggesting that the resulting nanofibres are much less crystalline than MCC. It would appear that the acid treatment causes significant damage to the crystalline regions of MCC, perhaps resulting from the hydrolysis time used. This observation is attributed to the low amorphous content of MCC and lack of protective layer (lignin and hemicelluloses). Thus, the crystallites were first attacked during the hydrolysis, resulting in a decrease in overall crystallinity [65].

The effect on crystallinity of flax fibres after increasing number of passes through the microfluidiser at 1800 bar was also studied by X-ray diffraction (Fig. 13). The crystallinity index (I_c) was estimated from Eq. 1 using the height of the 200 crystalline peak (at $2\theta = 22.6°$) and the minimum for amorphous material (I_{am}) between the 200 and 110 peaks (at $2\theta = 18°$) [67].

$$I_c = (I_{200} - I_{am}/I_{200}) \times 100 \quad (1)$$

It is apparent from these results that, in general, crystallinity of the flax fibres increased, with number of passes and applied shear through the microfibrillator (Fig. 13). This again resulted from removal of the amorphous regions, where the lignin and polyose layer such as hemicellulose surrounding the flax fibres, were first defibrillated.

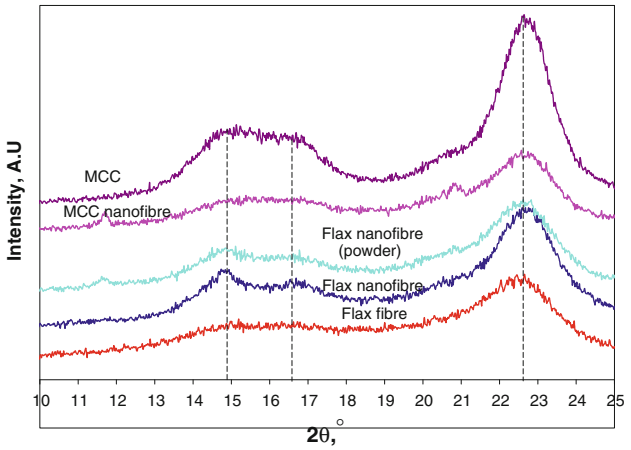

Fig. 12 X-ray diffraction patterns for cellulose nanofibres produced by acid hydrolysis and their unmodified flax and MCC controls

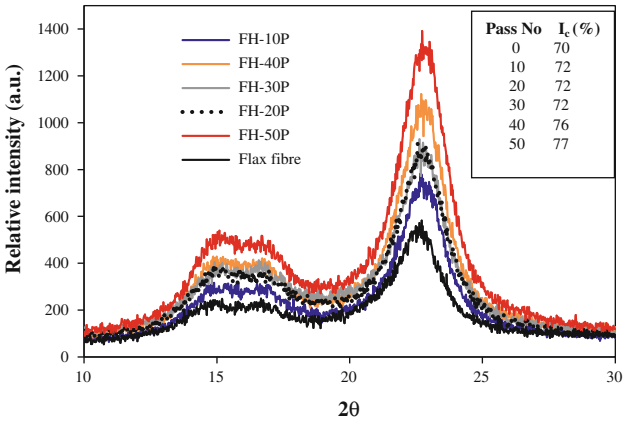

Fig. 13 X-ray diffraction patterns for the unmodified flax control and flax nanofibrils produced by multiple passes through microfluidiser M110-EHI at 1800 bar, including crystallinity index values

Thermal analysis

An understanding of how the structure and chemical composition of these materials affects their thermal decomposition is important during subsequent processing with polymers where aggressive heat and shear conditions can be experienced.

The thermal behaviour of cellulose nanofibres subjected to acid hydrolysis derived from the two different sources, is compared in Fig. 14, together with data for their host counterparts. Principal events observed from this analysis are given in Table 4. Compared to the original feedstocks, the thermal stability of cellulose nanofibres made by acid hydrolysis decreased significantly, in accordance with similar studies reported previously [55]. A single degradation peak was observed in the DTG curve of the source materials, while the cellulose nanofibres showed two degradation peaks. Also, the amount of char residue in flax nanofibre and MCC nanofibres was 33 and 39%, respectively, whereas in the feedstock source this was only 12% (MCC) and 22% (flax fibres). These effects originate from the sulphuric acid hydrolysis and the formation of acid sulphate groups on the cellulose nanofibres [68, 69], and catalysed dehydration promoting char formation [68–71]. The onset decomposition temperature of MCC and flax fibre was 280 and 210 °C, respectively. This reflects the presence of the less thermally stable non-structural hemicelluloses and pectin within the flax material. Hemicellulose is generally thought to decompose first, followed by cellulose and lignin [72–74].

TGA results for microfibrillated flax fibres, exposed to differing treatments and shear histories are summarised in Table 5. The degradation of unmodified flax fibre involves two main steps. The first step is the thermal depolymerisation of the hemicellulose and the cleavage of glycosidic linkages of cellulose while the second step is related to the decomposition of the levoglucosan [75, 76]. The effect of number of passes through the microfibrillator caused an increase in thermal stability for the cellulosic samples. This is thought to be influenced by the particle size, crystallinity and purity of the defibrillated flax fibrils. It was evident that increasing the number of homogenisation passes resulted in a decrease in particle size distribution and together with an increase in both cellulose purity and crystallinity, discussed earlier in relation to the DLS, FTIR and XRD results.

Figure 15 compares TG-MS evolution profiles for carbon dioxide and water during the pyrolysis before and after multiple passes through the microfluidiser, showing maximum signals for CO_2 and H_2O from the virgin flax fibres at 358 and 352 °C, respectively. A decrease in the intensity for the CO_2 signal occurred with increasing number of passes through the microfluidiser, together with a shift of these signals to lower temperatures. Increasing the number of passes, suppresses the flammability of the volatilisation products by raising the percentage of noncombustible compound (carbon dioxide). This is verified in the TG-MS in Fig. 15, where the maximum CO_2 MS secondary signal of sample (F-80P) appears 80 °C higher than for virgin flax fibres.

DTG curves of the silane treated nanofibres are illustrated in Fig. 16. The temperature of the first degradation peak for silane treated nanofibres (FS-5P to FS- 80P) is much higher than for untreated flax fibres (F-C), acid treated nanofibres (FA-5P to FA-80P) and alkali treated nanofibres (FN-5P to FN- 80P). Furthermore, increasing the number of passes also confers a significant improvement in thermal stability when the silane treatment is present. Rachini [63] also showed that the thermal stability of hemp fibres increased when modified with silane treatment.

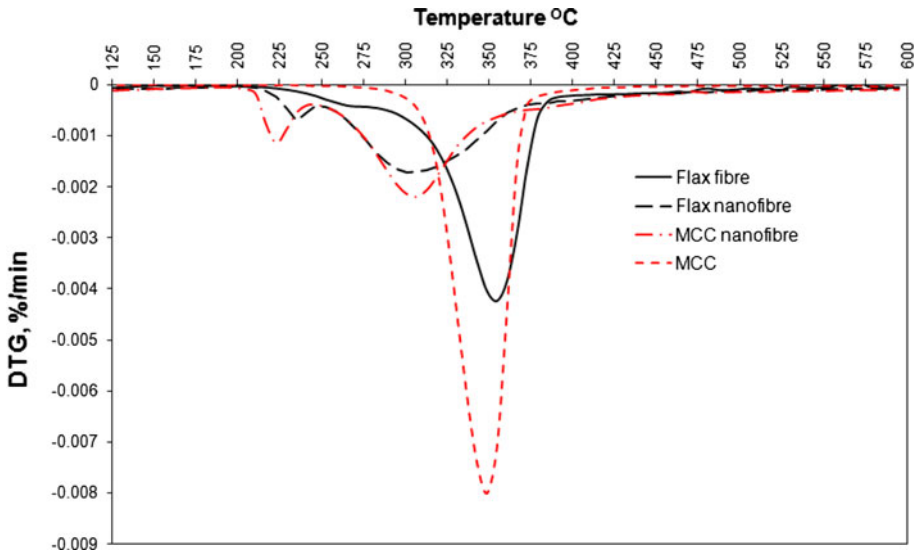

Fig. 14 DTG curves for flax and MCC and their corresponding nanofibres made by acid hydrolysis (under nitrogen)

Table 4 TG data of the cellulose sources and nanofibres

Material	Water content (%)	Char at 500 °C (%)	Onset temp (°C)	First stage		Second stage	
				T_{max} (°C)	Weight loss (%)	T_{max} (°C)	Weight loss (%)
MCC	3	12	280	–	–	349	86
MCC nanofibre	4	33	195	220	8	306	54
Flax fibre	7	22	210	–	–	358	71
Flax nanofibre	4	39	209	235	5	314	51

MCC nanofibre and flax nanofibre are the cellulose nanofibres derived from MCC, flax fibres with a length of between 20 and 30 mm and ground flax fibres, respectively, using acid hydrolysis

Table 5 A summary of TGA data for samples obtained using the microfluidisation process

Sample	Weight loss (%)			First degradation peak			Secondary degradation peak		
	1st step	2nd step	Residue	Area (%)	Height (mg/min)	Temperature (°C)	Area (%)	Height (mg/min)	Temperature (°C)
Flax control	73.15	16.62	10.23	64.49	0.25	348.79	10.75	0.029	499.46
F-5P	67.67	17.94	12.33	59.82	0.2	336.11	13.55	0.033	483.28
F-20P	60.56	25.59	12.34	56.39	0.2	335.86	19.55	0.038	483.19
F-50P	60.46	26.37	11.06	55.98	0.2	335.43	21.33	0.039	532.73
F-80P	57.43	30.8	11.11	51.3	0.21	332.64	24.04	0.042	566.9
FA-5P	73.67	14.84	11.49	63.46	0.23	343.75	7.35	0.02	467.08
FA-20P	64.96	25.88	9.16	57.3	0.23	349.25	18.18	0.039	497.54
FA-50P	64.63	24.58	10.7	57.69	0.23	344.33	17.94	0.045	491.89
FA-80P	62.51	26.38	10.94	56.74	0.22	340.6	19.2	0.034	493.59
FN-5P	78.15	11.77	9.9	69.83	0.31	355.46	6.45	0.023	474.25
FN-20P	74.55	13.85	11.6	66.42	0.26	347.18	7.97	0.026	462.96
FN-50P	69.8	19.08	11.1	62.18	0.24	353.08	12.18	0.029	498.58
FN-80P	65.5	24.1	10.08	58.46	0.2	342.61	15.92	0.031	493.59
FS-5P	63.44	–	36.56	56.67	0.08	404.76	–	–	–
FS-20P	57.94	–	42.06	53.54	0.078	408.5	–	–	–
FS-50P	68.11	–	31.89	62.1	0.085	411.82	–	–	–
FS-80P	58.4	–	41.6	53.54	0.072	418.63	–	–	–

Microfluidizer M-110Y at 1000 bar

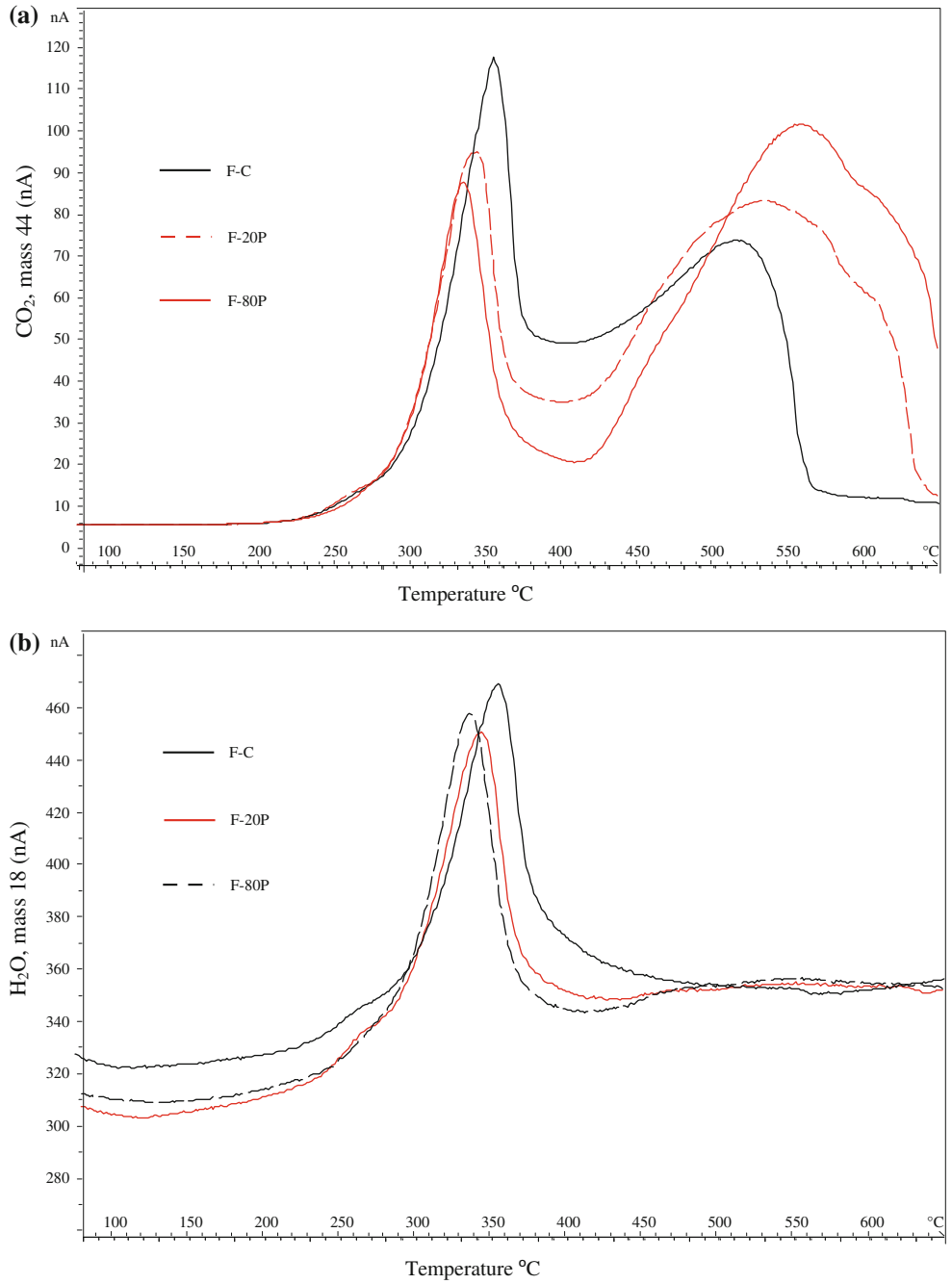

Fig. 15 TG-MS gas evolution profiles for flax control, and after 20 and 80 passes through microfluidiser M100-Y at 1000 bar. **a** Carbon dioxide, **b** water

Conclusions

Cellulose nanofibres and nanofibrils derived from MCC and flax fibres were characterised after preparation by two techniques: acid hydrolysis, combined with the application of ultrasound, and high pressure microfluidisation. The aspect ratio of nanofibres made by hydrolysis using sulphuric acid was around 17 for the two feedstocks studied, whereas material made by microfluidisation were orders of magnitude higher, depending on the extent of shear experienced (defined by the number of passes and pressure applied) and the form of feedstock pre-treatment used. In this regard, there was evidence from FTIR that 3-glycidoxypropyltrimethoxysilane chemically bonded to the nanofibril surface yielding finer fibres with reduced agglomeration. Furthermore, FTIR demonstrated that most hemicellulose and lignin was extracted during the acid hydrolysis process and after acid and alkaline pretreatment

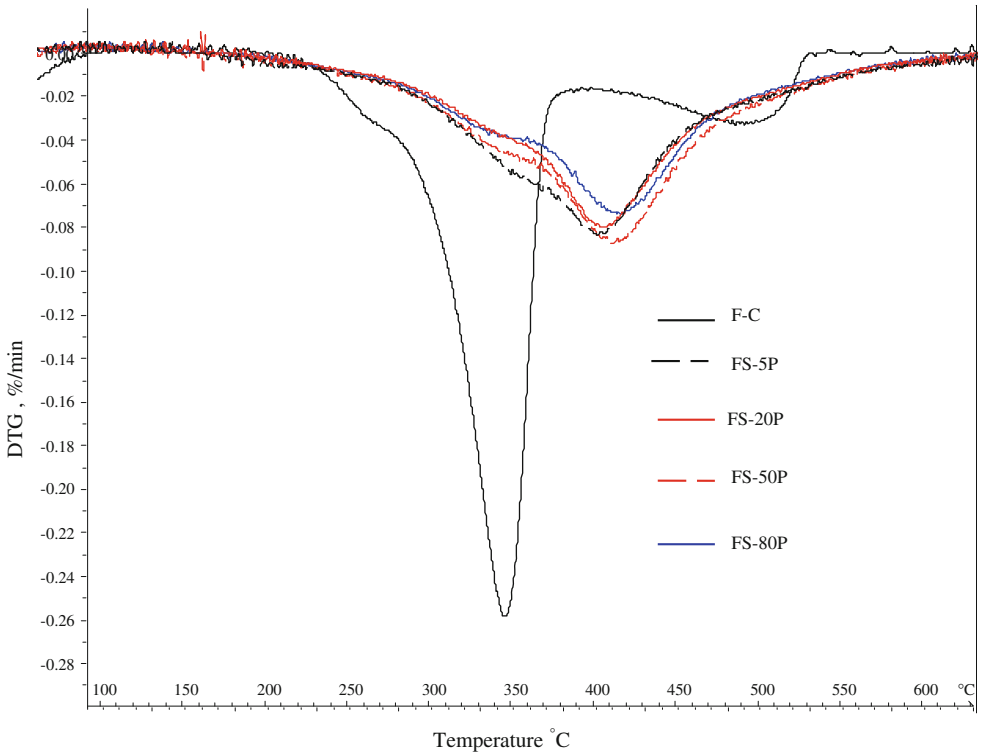

Fig. 16 DTG curves for flax and its corresponding nanofibrils (with silane pretreatment) produced by multiple passes through microfluidiser M110-Y at 1000 bar

prior to microfluidisation. It was also observed that hydrolysis with sulphuric acid resulted in esterification of hydroxyl groups on the cellulose. X-ray diffraction of the various cellulose nanofibres revealed that acid hydrolysis of MMC significantly reduced overall crystallinity, whereas compared to the flax precursor, this increased due to preferential degradation of the amorphous components leaving more crystalline cellulose nanofibres remaining. With multiple passes through the microfluidiser the crystallinity index of the flax fibres was found to increase. Whereas the parent feedstocks showed a single DTG peak, after acid hydrolysis the resulting cellulose nanofibres gave two thermal decomposition events. It was also evident that degradation of the nanofibres occurred at significantly lower temperatures and gave a much higher char residue, due to a catalysing effect of the acid sulphate groups present. In contrast, the thermal stability of the cellulose nanofibrils increased with number of passes through the microfluidiser, particularly with acid and alkali pretreated material, probably due to the removal of lower thermal stability components, such as xylans. However, when silane treatment was combined with microfluidisation a major enhancement in thermal stability was observed. In general, pre-treatment with acid is considered the better option for hydrolysis of cellulosic fibres, where hemicelluloses and pectin contents are low, however, for materials like flax with a wider ranging composition, an alkaline step can remove the residual wax and non-cellulosic components, better than acid alone. Both pre-treatments, are shown to increase the thermal stability of fibres, the effect being enhanced with increasing number of passes.

References

1. Eichhorn SJ et al (2010) J Mater Sci 45:1. doi:10.1007/s10853-009-3874-0
2. Oksman K, Mathew AP, Sain M (2009) Plast Rubber Compos Macromol Eng 38:396
3. Habibi Y, Lucia LA, Rojas OJ (2010) ChemRev 110:3479
4. Qua EH, Hornsby PR, Sharma HSS, Lyons G, McCall RD (2009) J Appl Polym Sci 113:2238
5. Qua EH, Hornsby PR (2011) Plast Rubber Compos Macromol Eng (in press)
6. Bhatnagar A, Sain M (2005) J Reinf Plast Compos 24:1259
7. Wang B, Sain M (2005) In: Oksman K, Sain M (eds) Chapter 13: ACS Symposium Series 938, p 187
8. Mathew AP, Chakraborty A, Oksman K, Sain M (2005) In: Oksman K, Sain M (eds) Chapter 9: ACS Symposium Series 938, p 114
9. Petersson L, Oksman K (2005) In: Oksman K, Sain M (eds) Chapter 10: ACS Symposium Series 938, p 132
10. Zimmermann T, Pöhlere E, Geiger T, Schleuniger J, Schwaller P, Richter IK (2005) In: Chapter 4: ACS Symposium Series 938, p 33
11. Lu YS, Weng LH, Cao XD (2006) Carbohydr Polym 63:198
12. Noorani S, Simonsen J, Atre S (2005) In: Oksman K, Sain M (eds) Chapter 14: ACS Symposium Series 938, p 209
13. Dinand E, Chanzy H, Vignon MR (1999) Food Hydrocolloids 13:275
14. Bondeson D, Kvein I, Okman K (2005) In: Oksman K, Sain M (eds) Chapter 2: ACS Symposium Series 938, p 10

15. Tanem BS, Kvein I, Van Helvoort ATJ, Oksman K (2005) In: Oksman K, Sain M (eds) Chapter 5: ACS Symposium Series 938, p 48
16. Marcovich NE, Bellesi NE, Aranguren MI, Auad ML, Nutt SR (2006) J Mater Res 21:870
17. Petersson L, Kvien I, Oksman K (2007) Compos Sci Technol 67(11–12):2535
18. Roman M, Winter WT (2004) Biomacromolecules 5:1671
19. Grunert M, Winter WT (2002) J Polym Environ 10:27
20. Dufresne A, Cavaille JY, Vignon MR (1997) J Appl Polym Sci 64(6):1185
21. Heux L, Chauve G, Bonini C (2000) Langmuir 16(21):8210
22. Habibi Y, Chanzy H, Vignon MR (2006) Cellulose 13:607
23. Lu Y, Weng L, Cao X (2006) Carbohydr Polym 63:198
24. Araki J, Wada M, Kuga S, Okano T (1998) Colloids Surf A 30:75
25. Beck-Candanedo S, Roman M, Gray DG (2005) Biomacromolecules 6:1048
26. Ranby BG (1949) Acta Chem Scand 3:649
27. Ranby BG, Ribi E (1950) Experientia 6:12
28. Kvein I (2007) Characterization of biopolymer based nanocomposites. Doctor of Philosophy Thesis, Norwegian University of Science and Technology
29. Dufresne A, Cavaille JY (1999) In: Imam SH, Greene RV (eds) ACS Symposium Series 723, p 39
30. Helbert W, Cavaillé JY, Dufresne A (1996) Polym Compos 17:604
31. Angles MN, Dufresne A (2000) Macromolecules 33:8344
32. Morin A, Dufresne A (2002) Macromolecules 35:2190
33. Dong XM, Revol JF, Gray DG (1998) Cellulose 5:19
34. Svagan A (2006) Bio-inspired polysaccharide nanocomposites and foams. Doctor of Philosophy Thesis, KTH Chemical Science and Engineering, Department of Fibre and Polymer Technology, Stockholm, Sweden
35. Turbak AF, Snyder FW, Sandberg KR (1983) J Appl Polym Sci 37:815
36. Herrick FW, Casebier RL, Hamilton JK, Sandberg KR (1983) J Appl Polym Sci 37:797
37. Nakagaito AN, Yano H (2005) Appl Phys A 80(1):155
38. Yano H, Sugiyama J, Nakagaito AN, Nogi M, Matsuura T, Hikita M, Handa K (2005) Adv Mater 17(2):153
39. Zimmermann T, Pohler E, Geiger T (2004) Adv Eng Mater 6(9):754
40. Taniguchi T, Okamura K (1998) Polym Int 47(3):291
41. Berglund L (2005) In: Mohanty AK, Misra M, Drzal LT (eds) Natural fibers, biopolymers, and biocomposites. Taylor & Francis Group, CRC Press, Boca Raton, FL, p 808
42. Gassan J, Bledzki AK (1996) Appl Macromol Chem Phys 236: 129
43. Bledzki AK, Gassan J (1999) Prog Polym Sci 24:221
44. Bismarck A, Mishra S, Lampke T (2005) In: Mohanty AK, Misra M, Drzal LT (eds) Natural fibers, biopolymers, and biocomposites. Taylor & Francis, Boca Raton, p 37
45. Kernaghan K, Sharma HSS, Whiteside L (2006) Enzyme Microb Technol 39:1373
46. Sano N, Naito M, Chhowalla M, Kikuchi T, Matsuda S, Iimura K, Wang H, Kanki T, Amaratunga GAJ (2003) Chem Phys Lett 378(1–2):29
47. Caulfield DF, Moore WE (1974) Wood Sci 6:375
48. Ganan P, Cruz J, Garbizu S, Arbelaiz A, Mondragon I (2005) Polym Compos 26(2):121
49. Lee JY, Kim JS, Hyeok AK, Lee K, Kim DY, Bae DJ, Lee YH (2005) J Nanosci Nanotechnol 5(7):1045
50. Magid L (1996) In: Brown W (ed) Light scattering principles and development. Clarendon Press, Oxford
51. Bera D, Johnston G, Heinrich H, Seal S (2006) Nanotechnology 17:1722
52. Provencher SW (1982) Comput Phys Commun 27:213
53. Provencher SW (1982) Comput Phys Commun 27:229
54. Verleye GAL, Roeges NPG, De Moor MO (2001) Easy identification of plastics and rubbers. Rapra Technology Limited, Shawbury
55. Paralikar S (2007) Poly(vinyl alcohol)/cellulose nanocomposite barrier films. Master of Science Thesis, Oregon State University, USA
56. Neevel JG, Mensch TJC (1999) ICOM Comm Conserv 2:528
57. Panaitescu DM, Donescu D, Bercu C, Vuluga DM, Iorga M, Ghiurea M (2007) Polym Eng Sci 47(8):1228
58. Tamada Y (2003) J Appl Polym Sci 87:2377
59. Gousse C, Chanzy H, Excoffier G, Soubeyrand L, Fleury E (2002) Polymer 43:2645
60. Ganan P, Cruz J, Garbizu S, Arbelaiz A, Mondragon I (2004) J Appl Polym Sci 94:1489
61. Bisanda ETN, Ansell MP (1991) Compos Sci Technol 41:165
62. Sreekala MS, Kumaran MG, Thomas S (1997) J Appl Polym Sci 66:821
63. Rachini A, Le Troedec M, Peyratout C, Smith A (2009) J Appl Polym Sci 112:226
64. Abdelmouleh M, Boufi S, Belgacem MN, Duarte AP, Ben Salah A, Gandini A (2004) Int J Adhes Adhes 24:43
65. Nisizawa K (1973) J Ferment Technol 51:267
66. Fan LT, Gharpuray MM, Lee YH (1987) In: Biotechnology monographs, vol 3. Springer-Verlag, Berlin
67. Teixeira EM, Pasquini D, Curvelo AAS, Corrandini E, Belgacem MN, Dufresne A (2009) Carbohydr Polym 78:422
68. Kim DY, Nishiyama Y, Wada M, Kuga S (2001) Cellulose 8(1):29
69. Wang N, Ding E, Cheng R (2007) Polymer 48:3486
70. Scheirs J, Camino G, Tumiatti W (2001) Eur Polym J 37(5):933
71. Julien S, Chornet E, Overend RP (1993) J Anal Appl Pyrol 27:25
72. Sefain MZ, El-Kalyoubi SF, Shukry N (1985) J Polym Sci 23:1569
73. Wielage B, Lampke T, Marx G, Nestler K, Starke D (1999) Thermochim Acta 337:169
74. Byrne CE, Nagle DC (1997) Carbon 35(2):259
75. Nair KCM, Thomas S, Groeninckx G (2001) Compos Sci Technol 61:2519
76. Albano C, González J, Ichazo M, Kaiser D (1999) Polym Degrad Stab 66:179